



ORIGINAL ARTICLE

Molecular mechanism of *CHRDL1*-mediated X-linked megalocornea in humans and in *Xenopus* model

Thorsten Pfirrmann^{1,†}, Denise Emmerich^{4,7,†}, Peter Ruokonen⁵,
Dagmar Quandt², Renate Buchen⁸, Björn Fischer-Zirnsak^{4,7}, Jochen Hecht^{4,6},
Peter Krawitz⁴, Peter Meyer¹⁰, Eva Klopocki¹¹, Sigmar Stricker^{7,12},
Ekkehart Lausch⁹, Barbara Seliger², Thomas Hollemann¹, Thomas Reinhard⁸,
Claudia Auw-Haedrich⁸, Bernhard Zabel⁹, Katrin Hoffmann³
and Pablo Villavicencio-Lorini^{3,*}

¹Institute of Physiological Chemistry, ²Institute of Medical Immunology and ³Institute of Human Genetics, Martin Luther University Halle-Wittenberg, 06112 Halle, Saale, Germany, ⁴Institute of Medical and Human Genetics, ⁵Department of Ophthalmology and ⁶Berlin-Brandenburg Center for Regenerative Therapies, Charité Universitätsmedizin Berlin, 13353 Berlin, Germany, ⁷Development and Disease Group, Max-Planck-Institute for Molecular Genetics, 14195 Berlin, Germany, ⁸Department of Ophthalmology and ⁹Center for Pediatrics and Adolescent Medicine, University Hospital of Freiburg, 79106 Freiburg, Germany, ¹⁰Department of Ophthalmology, University of Basel, 4056 Basel, Switzerland, ¹¹Institute of Human Genetics, Biocenter, Julius-Maximilians University Würzburg, 97074 Würzburg, Germany and ¹²Institute for Chemistry and Biochemistry, Freie Universität Berlin, 14195 Berlin, Germany

*To whom correspondence should be addressed at: Institute of Human Genetics, Martin Luther University Halle-Wittenberg, Magdeburger Str. 2, 06112 Halle (Saale), Germany. Tel: +49 3455574437; Fax: +49 3455574701; Email: pablo.lorini@uk-halle.de

Abstract

Chordin-Like 1 (*CHRDL1*) mutations cause non-syndromic X-linked megalocornea (XMC) characterized by enlarged anterior eye segments. Mosaic corneal degeneration, presenile cataract and secondary glaucoma are associated with XMC. Beside that *CHRDL1* encodes Ventroptin, a secreted bone morphogenetic protein (BMP) antagonist, the molecular mechanism of XMC is not well understood yet. In a family with broad phenotypic variability of XMC, we identified the novel *CHRDL1* frameshift mutation c.807_808delTC [p.H270Wfs*22] presumably causing *CHRDL1* loss of function. Using *Xenopus laevis* as model organism, we demonstrate that *chrdl1* is specifically expressed in the ocular tissue at late developmental stages. The *chrdl1* knockdown directly resembles the human XMC phenotype and confirms *CHRDL1* deficiency to cause XMC. Interestingly, secondary to this *bmp4* is down-regulated in the *Xenopus* eyes. Moreover, phospho-SMAD1/5 is altered and BMP receptor 1A is reduced in a XMC patient. Together, we classify these observations as negative-feedback regulation due to the deficient BMP antagonism in XMC. As *CHRDL1* is preferentially expressed in the limbal stem cell niche of adult human cornea, we assume that *CHRDL1* plays a key role in cornea homeostasis. In conclusion, we provide novel insights into the molecular mechanism of XMC as well as into the specific role of *CHRDL1* during cornea organogenesis, among others by the establishment of the first XMC *in vivo* model. We show that unravelling

[†] These authors contributed equally to this work.

Received: December 10, 2014. Revised and Accepted: February 13, 2015

© The Author 2015. Published by Oxford University Press. All rights reserved. For Permissions, please email: journals.permissions@oup.com

monogenic cornea disorders like XMC—with presumably disturbed cornea growth and differentiation—contribute to the identification of potential limbal stem cell niche factors that are promising targets for regenerative therapies of corneal injuries.

Introduction

X-linked megalocornea (XMC) [MIM309300] manifests as an inborn defect of the anterior eye segment characterized by a corneal diameter larger than 12.5 mm and a deep anterior eye chamber. XMC is therefore termed also anterior megalophthalmos and occurs without elevated intraocular pressure (IOP) (1,2). It is an important differential diagnosis for primary congenital glaucoma (IOP-associated buphthalmos) that leads to a high risk of vision loss and, thus, needs a fast diagnostic clarification and prompt treatment (3). Furthermore, XMC is classified as non-syndromic and has to be distinguished from megalocornea in the context of syndromes, e.g. neonatal Marfan syndrome or megalocornea-mental-retardation (MMR) syndrome [MIM249310] (4,5). Usually, XMC patients have mild to moderate myopia and some complain of photophobia and iridodonesis due to iris hypoplasia. Additional ocular anomalies can be arcus lipoides, mosaic corneal degeneration, pigment dispersion along the inner corneal surface (Krukenberg's spindle), cataract and lens dislocation (2). Although the IOP is primarily normal, megalocornea might predispose to secondary glaucoma due to a widened ciliary body and a potential pigment deposition in the trabecular meshwork (6,7).

Different mutations in the *Chordin-Like 1* (*CHRDL1*) gene have been identified as the disease causing genetic alteration in XMC (3,8,9). The initial finding was a 240 kb microdeletion on Xq23 encompassing the *CHRDL1* gene (9). Sequence analysis of further patients with megalocornea revealed missense, nonsense and frameshift mutations in the *CHRDL1* gene. *CHRDL1* encodes the protein Ventroptin, which is a bone morphogenetic protein 4 (BMP4) antagonist (10). As a member of the regulatory network of transforming growth factor-beta (TGF β) signaling, Ventroptin is involved in cell fate determination as well as in cell differentiation. *CHRDL1* is expressed in the anterior eye segment (cornea, lens, trabecular meshwork) and in the retina, starting in embryonic development and lasting into adulthood (9,10). It is also differentially expressed in fetal brain regions, with highest expression in the cerebellum and the neocortex (9). Overexpression experiments in embryonic chick retina showed a role of Ventroptin in patterning of retinotectal projections (10). In contrast, presumed loss of function mutations in humans revealed only mild cone system dysfunction in retinal electrophysiology and inter-hemispheric asymmetry in visual evoked potentials in one subject with a microdeletion encompassing the 3' end of *CHRDL1* (9). Although focal white matter volume reductions could be found in some patients with megalocornea, no clinical correlate was observed in the reported patients so far (9). Recently, in one patient, a *CHRDL1* missense variant has been detected in association with Neuhäuser syndrome, also known as MMR syndrome [MIM249310]. The authors postulate that this *CHRDL1* variant accounts for the eye phenotype and that the MMR syndrome, in some cases, might be di- or multigenic (3).

In the present study, we report on a novel *CHRDL1* frameshift mutation in a family with XMC. Moreover, we investigated the molecular mechanism underlying XMC and its phenotypic variability. By a knockdown approach, using *Xenopus laevis* (Xl) as the first model organism for XMC, we characterized the impact of *CHRDL1* deficiency on eye development. Furthermore, we revealed the influence on BMP signaling in Humans and *Xenopus*. Finally, our data suggest that *CHRDL1* (Ventroptin) is very likely a novel

limbal stem cell niche factor of the adult human cornea. These findings could contribute to regenerative approaches for the treatment of corneal lesions, as advances in cornea regeneration concepts by targeting limbal stem cell niche factors are becoming reasonable therapeutic options for allogeneic transplantation (11,12).

Results

XMC shows a broad intrafamilial phenotypic variability regarding biometric abnormalities and associated ocular anomalies

The index patient (IV-1), first son of non-consanguineous healthy parents, was born at 40 weeks' gestation after uncomplicated pregnancy with remarkably large eyes reminding of buphthalmos (Fig. 1A). Instant diagnostic efforts were made to exclude primary congenital glaucoma and to prevent visual loss of the patient. However, this suspected diagnosis was discarded due to normal IOP. Since no other organ anomalies were detected, a syndromic condition seemed not to be likely. In follow-up examinations, no progression of the eye phenotype was noted and the patient developed age-based with regard to motor and mental function.

The family history of the patient was positive for enlarged eyes and pedigree analysis suggested a X-chromosomal recessive inheritance. Four affected males related to each other by obligate carrier females could be identified and no male-to-male transmission was observed (Fig. 1B). Altogether, the clinical history of our index patient IV-1 and the pedigree analysis enabled us to diagnose non-syndromic XMC, a rare genetic eye disorder. The deceased great-grandfather I-1 of patient IV-1 had been the first family member with obvious XMC phenotype. Moreover, he had undergone bilateral cataract surgery at age of ~56 years and had developed loss of corneal transparency at age of 85 years probably due to decompensation of corneal endothelium. Furthermore, he had a restricted peripheral vision field on both sides probably due to glaucoma, but retrospectively IOP values and optic nerve findings were not available to verify this assumption. Consistent with the X-chromosomal recessive inheritance, none of his sons and daughters was described as being affected. From the second, third and fourth generation of our study family, we were able to perform ophthalmic investigations of two further affected males (III-5, III-8), besides the index patient IV-1, who was by now 14 years old, and some of the healthy brothers (III-3, IV-2) as well as obligate carrier females (II-2, III-1).

The patients IV-1 and III-5 showed spherical refraction anomalies on both eyes ranging from -1.5 to -2.5 dioptres revealing mild myopia. Horizontal corneal diameters of these patients were at 16 mm and 14.5 mm, whereas the corneal diameters of their unaffected brothers III-3 and IV-2 were normal at 12 mm (normal range 11–12.5 mm), respectively (Fig. 1C). The lateral corneal profiles of the affected males III-5, III-8 and IV-1 appeared pre-bulged. Although the index patient IV-1 showed a dome-shaped cornea, the lateral aspects of the corneas of III-5 and III-8 appeared to be keratoconus-like. The obligate carrier females II-2 and III-1 as well as the unaffected male sibling IV-2 of the index patient IV-1 revealed flat corneas (Fig. 1D).

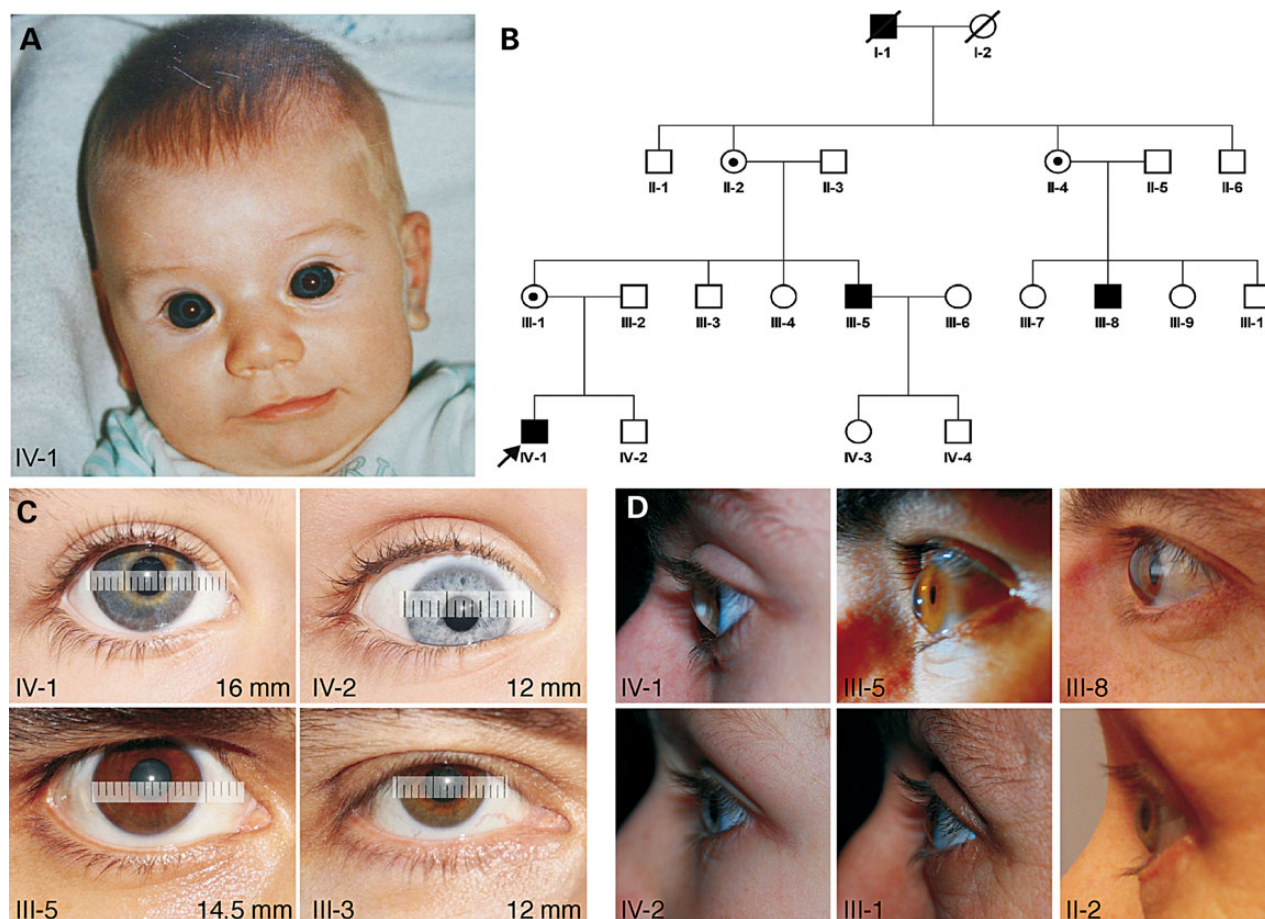


Figure 1. Family with XMC revealing the intrafamilial phenotypic variability. (A) Index patient (IV-1) with bilateral megalocornea at age of 2 months. (B) Pedigree of the study family revealing an X-linked inheritance pattern of megalocornea. (C) Corneal diameters of the index patient at age of 14 years (IV-1) and his affected uncle (III-5) compared with their non-affected brothers (III-3, IV-2). (D) Corneal profiles from the lateral view comparing affected males (IV-1, III-5, III-8) with obligate carrier females (II-2, III-1) and non-affected male relative (IV-2).

By optical interferometry, we determined elevated ratios of anterior chamber (AC) depth versus axial length (AL) being at 0.26 in patient IV-1 and 0.20 in patient III-5 (Fig. 2E). In contrast, the AC/AL ratios in the unaffected relatives ranged from 0.13 to 0.16. Slit lamp examinations confirmed a very deep anterior eye chamber of patient IV-1 compared with his unaffected brother IV-2 (Fig. 2C and D).

Consistent with a non-progressive isolated anterior megalophthalmos, an underlying glaucoma could be excluded in patient IV-1 once again at the age of 14 years. His IOP was not elevated (Fig. 2I) nor did the Heidelberg Retina Tomography (HRT) confocal laser scanning display a pathologic cupping of the optic nerve head (Fig. 2G and H). Corneal pachymetry indicated a reduced corneal thickness up to 350 μm at the corneal apex of patient IV-1. The corneal apex thickness of patient III-5 was decreased up to 405 μm in comparison with his unaffected brother III-3, showing 471 μm (Fig. 2F). In addition, patient III-8 had also a reduced corneal thickness, but despite this, he was treated for myopia by laser-assisted surface ablation elsewhere and he suffered from severe pain postoperatively. Although patient IV-1 exhibited the most apparent anterior megalophthalmos in comparison with the other affected males, he did not have further ocular anomalies, e.g. congenital cataract. Instead, XMC-associated complications were reported in the patients I-1, III-5 and III-8: as mentioned before, patient I-1 underwent

cataract surgery early in his fifth decade of life, whereas patient III-8 needed surgical lens removal and implantation of an artificial intraocular lens even earlier in his third decade of life because of congenital cataract. Furthermore, patient III-8 suffered from spontaneous retinal detachment on the right eye due to a vitreous degeneration, but vision loss could be prevented by immediate surgical intervention. Patient III-5 exhibited congenital cataract and iris hypoplasia accompanied with transillumination and intraocular straylight causing moderate photophobia. Moreover, patient III-5 had iridodonesis, mild displacement of the pupils, slight arcus lipoides and Krukenberg's spindle pigment dispersion at the inner corneal surface (Fig. 2A and B).

Novel hemizygous *CHRD1* frameshift mutation results in a premature termination codon causing reduced *CHRD1* mRNA levels in patient-derived cells

To screen for disease causing mutations in the recently identified candidate gene *CHRD1* or possible other unknown X-chromosomal candidate genes for megalocornea, a DNA sample of patient III-5 was analysed by next-generation sequencing after targeted enrichment of the X-chromosomal exome. This analysis yielded raw sequence data for the exons of the target region on X-chromosome comprising 610 kb. 517 kb of this region was covered by more than 10 reads, and 498 sequence variants were

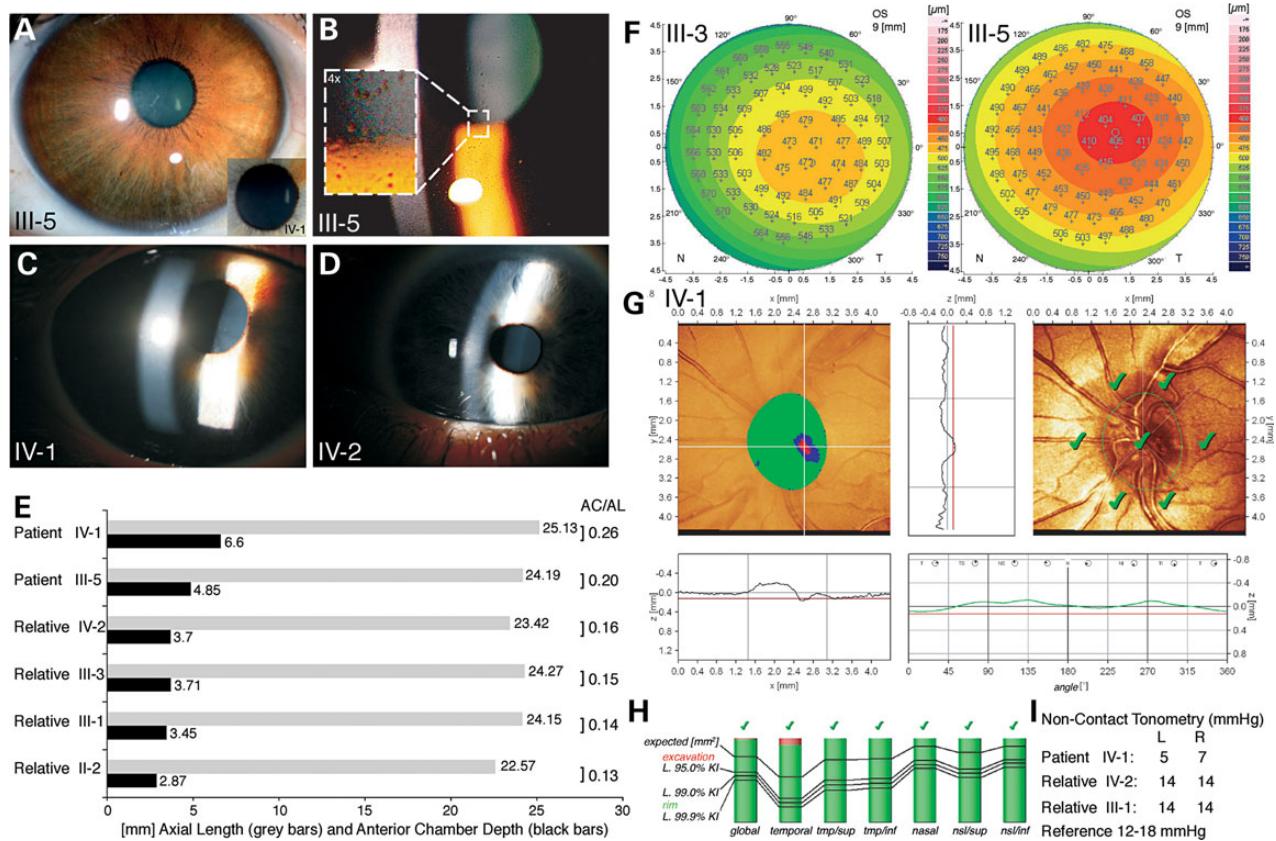


Figure 2. Distinctive phenotypic features of XMC. (A) Slit lamp findings in affected male III-5, indicating ectopia pupillae and congenital cataract (B) as well as the pigment dispersion (Krukenberg spindle) on the inner corneal surface. Note the cataract of patient III-5 is difficult to see, for better comparison, a cutout photograph of the clear lens of patient IV-1 was added. (C) Deep AC of the eye in patient IV-1 compared with his (D) non-affected brother IV-2. (E) AC and AL of the eyes from patient IV-1 and III-5 compared with their non-affected brothers (IV-2, III-3) and their mothers (II-2, III-1). (F) Corneal pachymetry of central corneal region (9 mm in diameter) of patient III-5 (right) and his non-affected brother (left). Color code indicates values around 400 μm or beneath in red, and values around 425 μm and above in orange up to blue. (G) HRT confocal scanning laser ophthalmoscopy of patient IV-1, indicating a normal optical nerve papilla. In the 2D color coded topography map, neutral null plane is marked in green, recession up to 0.1 mm in blue, excavation with more than 0.1 mm in red, also visualized in the profiles of orthogonal sections. (H) Comparison of the optical nerve papilla excavation values of patient IV-1 with references according to Moorefield's classification. (I) Non-contact tonometry (mmHg) reveals no elevated IOP of patient IV-1.

detected with SAMtools. Further filtering of the sequence variants by GeneTalk resulted in seven variants of unknown clinical significance including a hemizygous two basepair deletion (c.807_808delTC) in exon 9 of the *CHRDL1* gene (Fig. 3A). This deletion causes a frameshift mutation leading to a substitution of histidine to tryptophane at codon 270, and a premature termination codon 22 amino acids downstream (p.H270Wfs*22). We validated the identified *CHRDL1* mutation by Sanger sequencing and showed that the allele segregates with the phenotype in the study family (Fig. 3B) confirming a X-chromosomal recessive inheritance pattern: the same mutation was detected in all other affected males (III-8 and IV-1) and in the asymptomatic obligate carrier females, showing a hemizygous or a heterozygous genotype, respectively. Non-affected male siblings did not carry the *CHRDL1* frameshift mutation. We characterized the mutational effect by reverse transcriptase-polymerase chain reaction (RT-PCR) analysis of *CHRDL1* mRNA extracted from mononuclear (MNC) and polymorphonuclear (PMN) cells obtained from patient III-5 and a control (Fig. 3C) as well as from patient IV-1 and his healthy brother VI-2 (Supplementary Material, Fig. S1). The mutant *CHRDL1* mRNA was markedly reduced in MNC and completely missing in PMN of the patients when compared with healthy controls.

Knockdown of *chrd1* in *Xl* recapitulates the human XMC phenotype and influences *bmp4* expression

To prove that the XMC typical phenotypes are caused by *CHRDL1* loss of function, we used the African clawed frog *Xl* as a model organism. First, we determined the temporal expression of *chrd1* in *Xl* at consecutive developmental stages by RT-PCR. No *chrd1* transcript was traceable at early stages, whereas expression was detectable at Nieuwkoop and Faber (NF) stage 30 until the latest stage analysed (NF stage 42; Fig. 4A). This result was corroborated by whole mount *in situ* hybridization (WMISH) with *chrd1*-specific probes and showed a signal only in late stage embryos (NF stage 37; Fig. 4B). No staining was detectable at earlier stages (not shown). We observed *chrd1* expression in the optic cup, the lens and the ciliary marginal zone indicating a specific role of *CHRDL1* during eye development. In addition, the otic vesicle, the ependymal layer of the ventricle system and the notochord were strongly positive for *chrd1* transcript signal.

To induce a *chrd1* loss of function in *Xenopus*, we established a morpholino (MO) knockdown using a mixture of two different MO anti-sense oligonucleotides (MO1 + 2) directed against the splice sites of *chrd1* exon1/intron1 or intron1/exon2. We performed the MO1 + 2 injection experiments in the 2-cell stage of *Xl* to reach an

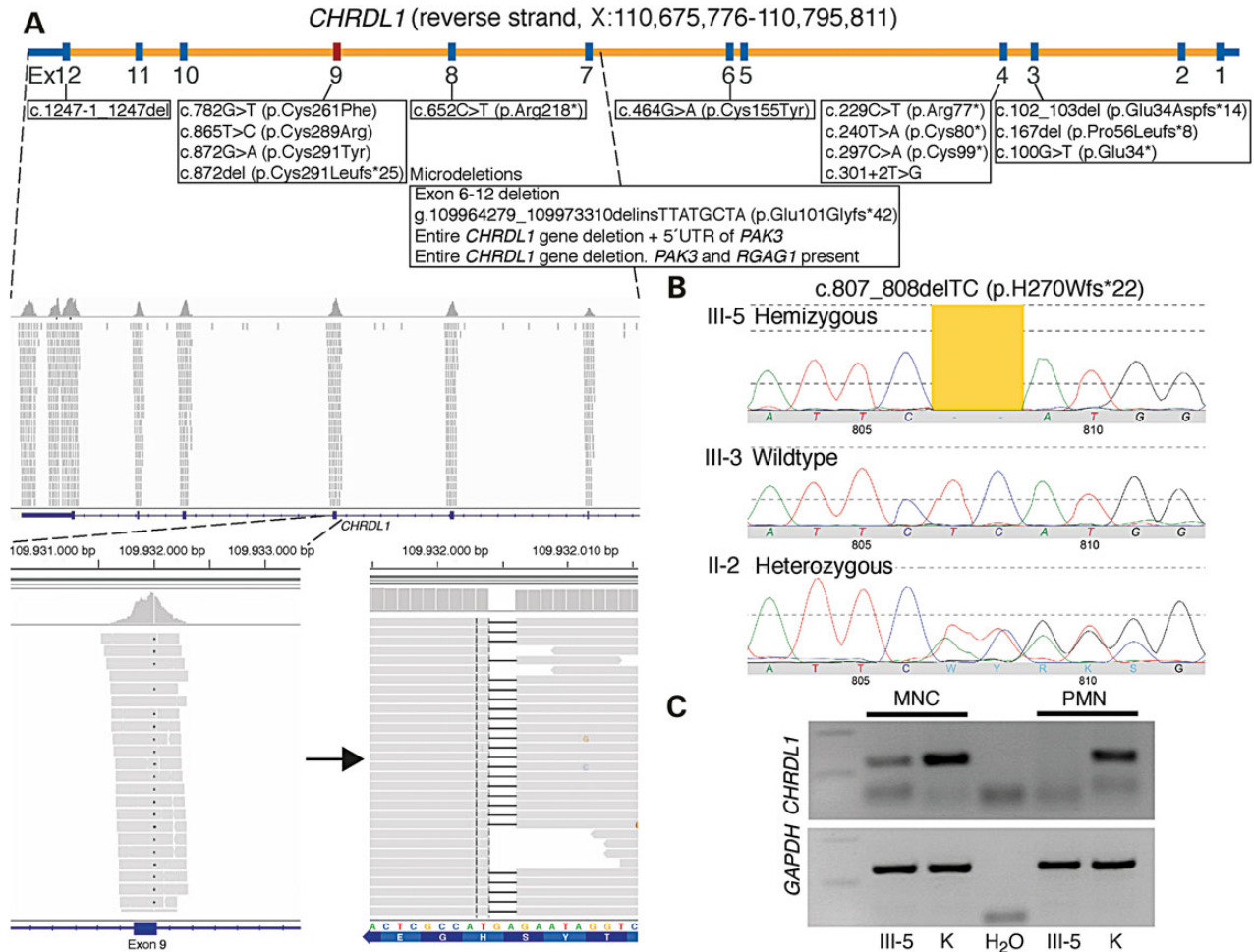


Figure 3. Novel *CHRDL1* frameshift mutation resulting in reduced mRNA levels. (A) Overview of previously described *CHRDL1* mutations and alignment of sequence reads after X-chromosomal exome sequencing by IGV browser. Depicted is a part of the *CHRDL1* locus Xq23. Boxes indicate magnifications of *CHRDL1* exon 9 that harbors the 2-base pair deletion. Note that *CHRDL1* is located on the reverse strand of the X-chromosome; therefore, the reverse complement sequence is shown. (B) Representative results of segregation analysis by Sanger sequencing of *CHRDL1* exon 9 in the study family, showing hemizygous, heterozygous or wild-type genotype for affected males, asymptomatic carrier females or non-affected males, respectively. (C) Semi-quantitative RT-PCR analysis of *CHRDL1* mRNA levels in affected male III-5 and control.

efficient knockdown. As *chrdl1* interferes in early developmental stages with *bmp4* and influences body patterning, we desisted from rescue experiments by simultaneous *chrdl1* overexpression (10). As shown by RT-PCR analysis (Fig. 5E), the application of MO1 + 2 efficiently repressed *chrdl1* splicing in treated embryos. Figure 5A shows representative photographs of stage 42 embryos. Phenotypic alterations caused by *chrdl1* MO1 + 2 injection include changes of the eye size, mainly enlargement and, in addition, coloboma (Fig. 5A and B). As indicated, some embryos revealed pre-bulging of the lens and cornea, similar to the dome-shaped cornea in XMC patients. Histological sections demonstrated that XI, in contrast to the human eye, reveals only a single eye compartment at least at tadpole stage. This may explain the enlargement of the whole eye instead of just the anterior part (Fig. 5C). Interestingly, the pupil and lens of the MO-treated XI eye appeared to be slightly ectopic, a feature also observed in XMC patients with regard to the pupil (Figs 1C and 2A).

From three clutches, 81% of *chrdl1* MO1 + 2 injected embryos showed an alteration of the eye's structure, compared with 19% of standard MO-injected controls (total number of embryos $n = 384$) (Fig. 5B). Statistical analysis confirmed the correlation of the eye phenotypes observed with *chrdl1* MO1 + 2 injection ($P < 0.001$; χ^2 -test). Next, average eye diameters were measured

and compared between the *chrdl1*-injected site (is) and the non-injected site (nis) (Fig. 5C and D). Interestingly, we observed a statistically significant increase in the eye's size when *chrdl1* function was suppressed ($P = 0.0028$, one-tailed t-test). We measured an increase in the average eye diameter from 477 to 515 μm at NF stage 42 ($n = 9$).

CHRDL1 interacts with BMP4 in vertebrates (10,13). To investigate the correlation of *chrdl1* and *bmp4* in the XI XMC model, we performed WMISH using a *bmp4*-specific probe in *chrdl1* MO-injected embryos (Fig. 6A). Similar to *chrdl1*, *bmp4* is specifically expressed in the ocular and periorcular regions. Additionally, we detected strong expression in the otic vesicle and to a broader extent in the ventricular zone of the forebrain. In contrast to the *chrdl1*, the lens expresses *bmp4* at a much lower level. *Bmp4* expression appears to be reduced on the *chrdl1* MO-injected side, especially in the ventral ocular and periorcular region as well as in the otic vesicle (Fig. 6B).

Altered BMP signaling in association with *CHRDL1* mutation

To determine whether the *CHRDL1* mutation of our XMC patients influences the BMP pathway, intracellular phospho-SMAD1/5 was quantified in lymphoblastoid cell lines (LCLs) by flow cytometry

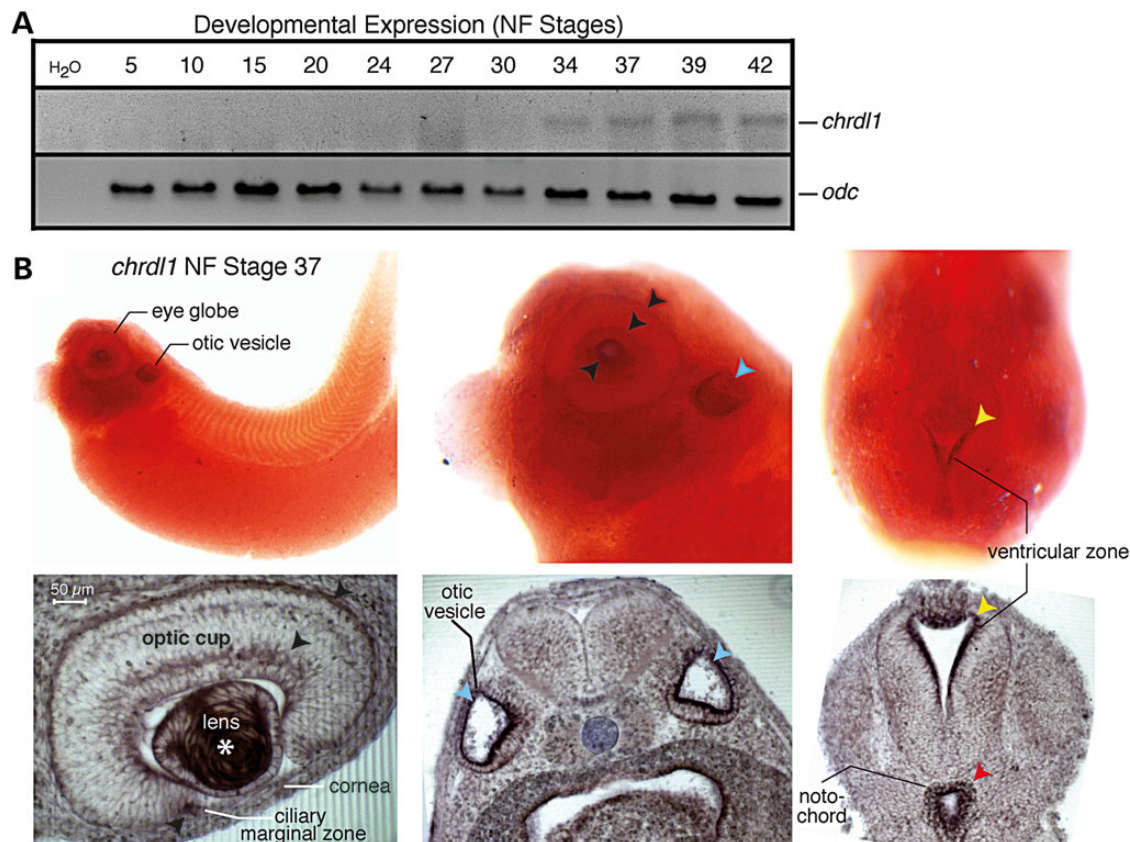


Figure 4. *Chrdl1* expression in XI displays a phylogenetic conserved function for eye development. (A) Temporal RT-PCR analysis of *chrdl1* expression (top panel); different developmental stages indicated at the top. *Odc* functions as RNA input control (bottom). (B) Spatial analysis of *chrdl1* expression. Whole mount in situ hybridization (WMISH) of wild-type XI embryos at NF stage 37 (top panel) and corresponding sections (bottom panel). Expression of *chrdl1* in the lens (white star), the optic cup (black arrows), the otic vesicle (blue arrow), the ependymal layer of the ventricle system (yellow arrow) and the notochord (red arrow).

as functional read-out for BMP signaling activity. Under unstimulated conditions, we measured a slightly higher level of intracellular phospho-SMAD1/5 in LCLs of patient IV-1 (Δ MFI: 133) when compared with LCLs obtained from his healthy brother VI-2 (Δ MFI: 81) (Fig. 7A). In contrast, BMP2/4 stimulation caused an increased phospho-SMAD1/5 induction in LCLs from the healthy brother IV-2 (Δ MFI: 534) compared with LCLs from patient IV-1 (Δ MFI: 300) (Fig. 7B). This correlates with less abundance of BMP receptor 1A (BMPRI1A) on the cellular surface (Fig. 7C) as well as in the intracellular compartment (Fig. 7D) of LCLs from patient IV-1 (Δ MFI: 19 and Δ MFI: 5510, respectively) compared with LCLs from his healthy brother IV-2 (Δ MFI: 62 and Δ MFI: 7422).

CHRD1 (Ventropin) is expressed like a limbal stem cell niche factor in adult human cornea

Immunohistochemistry of the CHRD1-encoded protein and BMP4 on healthy human cornea samples from anatomical sections revealed an almost mutual exclusive pattern of CHRD1 and BMP4 proteins, especially in the corneal epithelium (Fig. 8A). Although BMP4 is uniformly distributed over the whole corneal epithelium, CHRD1 is markedly expressed in the basal epithelium with a high-low expression gradient from the limbal stem cell niche to the mid corneal region. Additionally, the CHRD1 protein signal is enhanced in stromal keratocytes of the limbus with fading levels centripetally. In contrast, BMP4 is expressed to a lesser extent in corneal stroma. Both proteins are strongly expressed in the corneal endothelium as well.

Discussion

Based on the finding of a novel CHRD1 frameshift mutation in a large family with XMC, we initiated a comprehensive investigation to understand the molecular mechanism. By clinical assessment and segregation analysis, we show that the CHRD1 mutation is fully penetrant, but the broad intrafamilial phenotypic variability is challenging with respect to an appropriate medical management and prognostic estimation: first, clinical signs of XMC can be overlooked in newborns or be misdiagnosed as primary congenital glaucoma, leading to unnecessary sedation for the IOP measurement. Second, the severity of biometric abnormalities does not correlate with congenital cataract or pigment dispersion. Third, spontaneous retinal detachment due to vitreous degeneration has to be considered (14). Therefore, a robust genetic testing is important for early diagnosis and adequate patient care (Table 1).

The identified CHRD1 mutation in our study family confirms the homogeneous genetic origin of XMC (3,8,9). It emphasizes the pathomechanistic role of the TGF β signaling, which has also been found in connective tissue disorders associated with megalocornea, e.g. Marfan syndrome (5). The autosomal-recessive type of megalocornea with marfanoid habitus and zonular weakness [MIM251750], caused by genetic alterations in the *Latent transforming growth factor-beta-binding protein 2* (LTBP2) [MIM602091], is associated with the same pathway (15,16).

The CHRD1 frameshift mutation in our patients leads to a premature stop codon presumably resulting in decreased CHRD1 mRNA levels. One frequently used mechanism to abolish

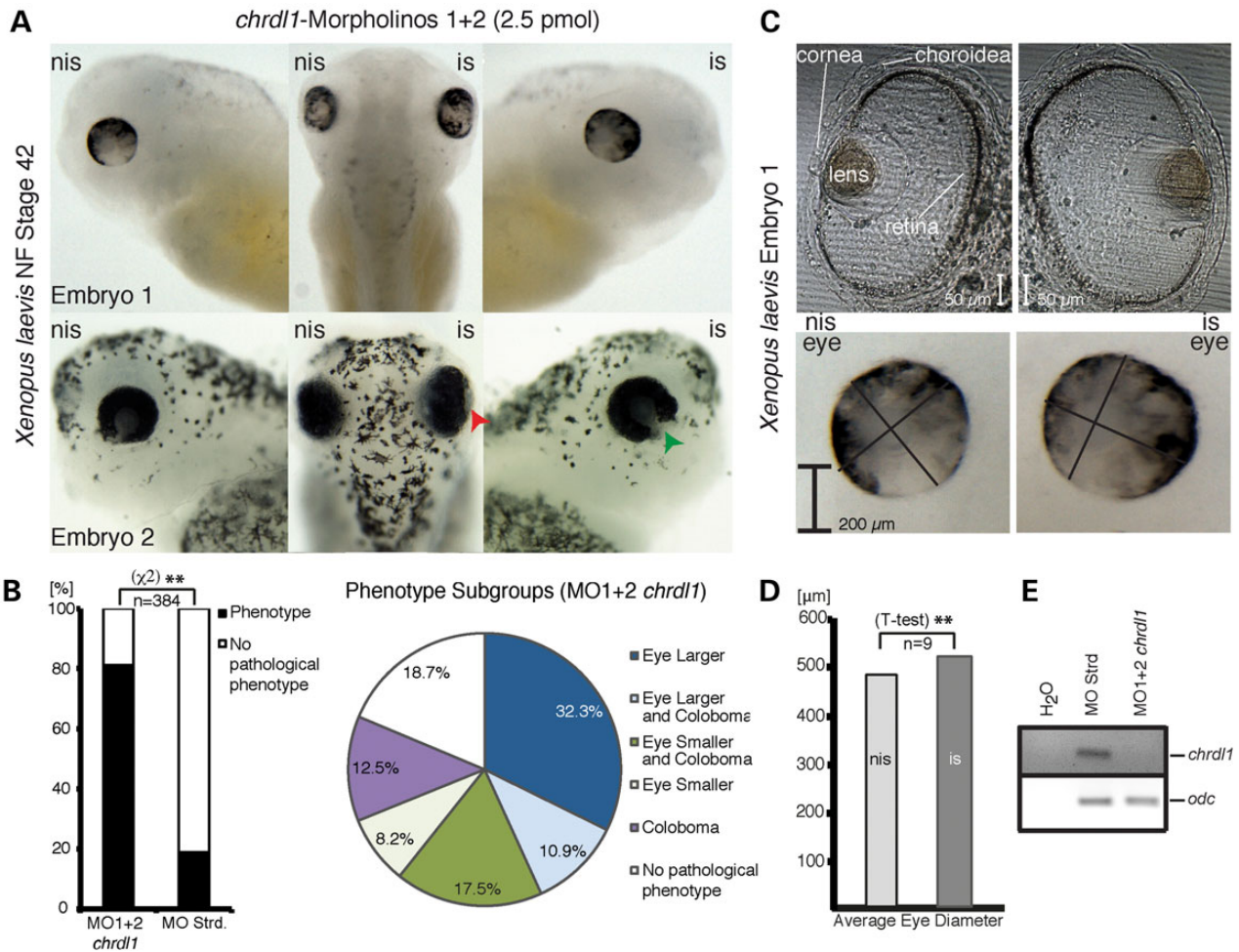


Figure 5. Knockdown of *Chrdl1* in XI recapitulates the human XMC phenotype. (A) Phenotype of XI embryos injected with a mixture of *chrdl1* MOs (MO1 + 2) or standard MO into one blastomere of 2-cell stage embryos grown to NF stage 42. is, injected side; nis, non-injected side; Strd, standard. green arrow, coloboma; red arrow, pre-bulged lens. XI can differ in skin pigmentation. (B) Respective phenotypes are quantified and presented as a bar graph in percent (%) (black, phenotype; white, no pathological phenotype); double asterisk indicate the statistical significance calculated by the χ^2 test. Phenotype subgroups are presented as a pie chart (right); for phenotypic subgroups of standard MO, see Supplementary Material, Figure S2. (C) Histomorphological and biometrical acquisition of XI eyes. Shown are plan view magnifications of injected versus non-injected eyes with two diameters (measured orthogonal to each other). (D) Bar graphs of the average eye diameter (μm) with statistical analysis (one-tailed t-test). (E) Semi-quantitative RT-PCR analysis measuring the MOs MO1 + 2 induced *chrdl1* knockdown efficiency.

non-functional mRNA molecules is nonsense-mediated RNA decay (NMD) (17,18). Indeed, we measure complete loss of *CHRDL1* mRNA in PMN cells and mRNA reduction in MNC cells. Therefore, as reported for most XMC-associated *CHRDL1* mutations, we assume a *CHRDL1* loss of function as the underlying molecular mechanism. On the one hand, cell type-specific differences in NMD efficiency are known (18), which could explain the different degrees of *CHRDL1* mRNA reduction observed in different cells of our patients. On the other hand, the known *CHRDL1* transcripts could differ in their stability, since they vary in their 3' UTR or possibly in their transcriptional rate depending on cell type. The abundance of different transcripts in the cell types could also explain the difference in the level of *CHRDL1* mRNA reduction. In MNCs, the resulting truncated protein, containing only two of the three cysteine-rich highly conserved von Willebrand factor, type C domains (VWFC), with BMP binding affinity, should have a reduced antagonistic effect on BMP4. So far, 13 from 19 currently described *CHRDL1* mutations cluster to the VWFC domains. Most of them lead to premature stop codons at the beginning of the coding sequence and should effectively be null mutations due to NMD

(3). Two whole gene deletions support the assumed *CHRDL1* loss of function mechanism in XMC. Regarding the broad phenotypic variability of XMC, even in an intrafamilial setting, an interfamilial genotype-phenotype correlation with respect to ocular and most probably subclinical non-ocular organ manifestations is quite challenging and remains to be elucidated. It is not yet fully understood how *CHRDL1* mutations can cause an eye-specific phenotype, although it is widely expressed in different tissues (9,10,13,19). Among others, the functional outcome of the mutation (loss versus gain of function), the co-expression with redundant BMP antagonists (e.g. *CHRD*) in certain tissues and the above-mentioned cell type-dependent NMD efficiency or RNA stability should play an important role in the organ-specific manifestation.

According to the currently prevailing model, cornea growth is achieved by differentiation of limbal stem cells during eye development (20,21). Therefore, we postulate that XMC results from premature cornea development due to accelerated growth and differentiation of limbal stem cells by an imbalanced *CHRDL1*-BMP4 antagonism in favor of BMP signaling and vice versa in

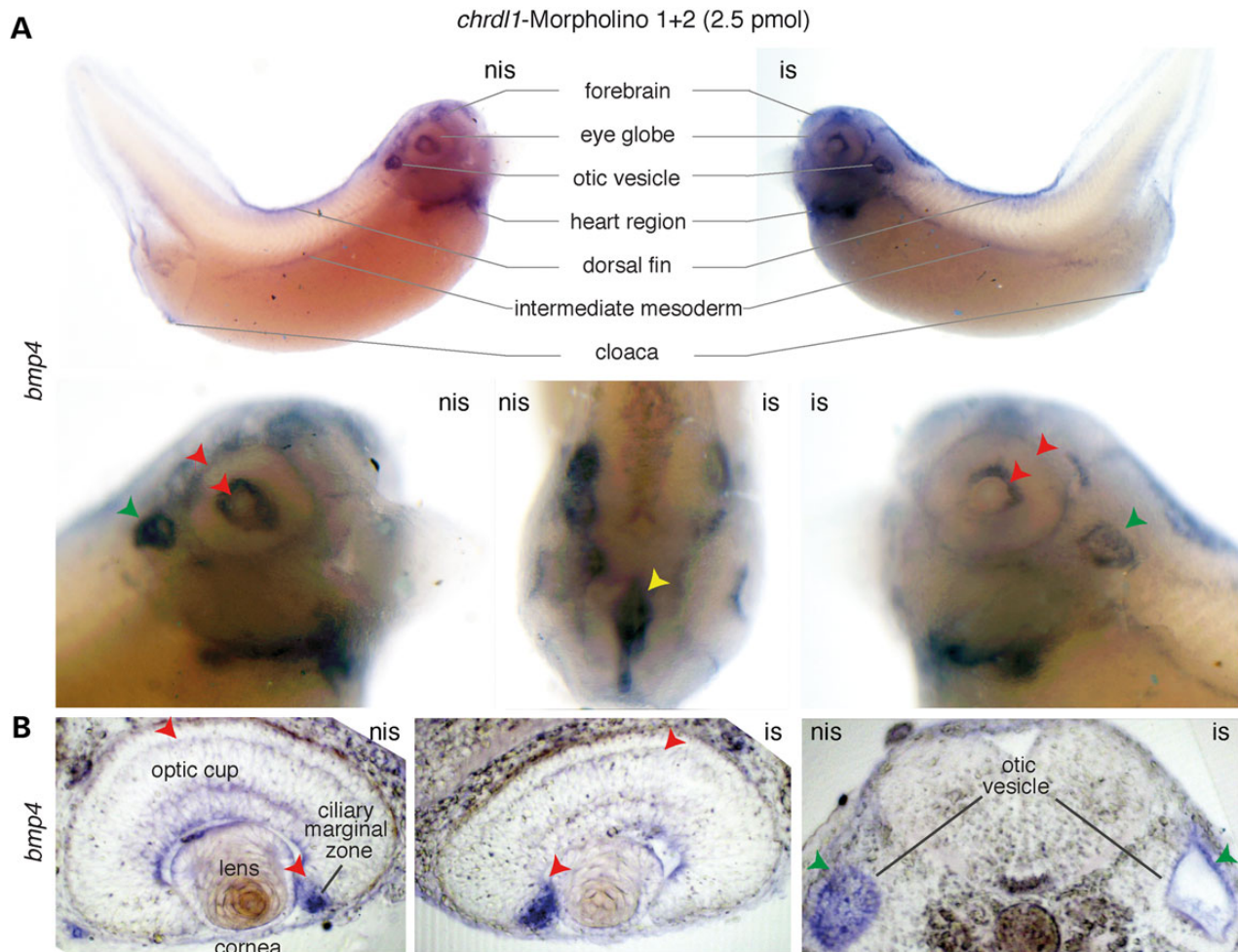


Figure 6. *Chrdl1* knockdown influences *bmp4* expression in XI. (A) *Chrdl1* MOs MO1 + 2-injected embryos (NF stage 37) were used for *in situ* hybridization with *bmp4* as a marker probe. is, injected side; nis, non-injected side. Expression of *bmp4* in the optic cup (red arrows), the otic vesicle (green arrow) and the ependymal layer of the ventricle system (yellow arrow) in the embryo (A) and its corresponding sections (B).

the case of microcornea (Fig. 8B). Consistent with this hypothesis, *BMP4* loss of function is known to cause microcornea in the form of syndromic microphthalmia type 6 (MCOPS6; MIM607932) (22,23). To prove our hypothesis, we established the first *in vivo* XMC model using a knockdown approach in XI. Until now, only the impact of *chrdl1* overexpression was tested on XI development. These results demonstrate that *chrdl1* similar to *chordin* is able to induce secondary axis formation after mRNA injection (10). We show that the suppression of *chrdl1* function induces eye phenotypes in the *Xenopus* tadpole that resemble the human XMC phenotype, i.e. larger eyes with specific findings in the anterior eye segment. Together with the spatiotemporal expression of *chrdl1* at tadpole stages, we give compelling evidence that *chrdl1* plays a conserved role during eye development. We therefore speculate that *chrdl1* knockdown in XI induces accelerated ocular growth. Our additional finding of pathologically widened coloboma has not previously been reported for the phenotypic spectrum of XMC. Thus, we propose that *CHRD1* gene analysis should be considered for patients with iris coloboma. Interestingly, the mild ectopic pupils observed in XMC patients can be the result of a mild variant of iris fissure closure. This observation is consistent with the association between coloboma and loss of function of *Smoc1* (SPARC-related modular calcium binding 1),

another BMP antagonist, in gene-trap mice (24). Furthermore, we observe a difference between *chrdl1* and *bmp4* expression levels in the lens of XI. We speculate that *CHRD1* physiologically prevents the development of cataract by preserving either a metabolic or structural homeostasis to maintain the transparency of the lens. Additionally, we are the first to report on *chrdl1* expression in the otic vesicle and the ependymal layer of the cerebral ventricular system. A possible clinical relevance of these findings remains to be elucidated in XMC patients.

The establishment and preservation of stable developmental gradients appears to require multiple mechanisms to balance agonistic and antagonist effects on BMP signaling. Consistent with this theory, we observe a down-regulation of *bmp4* expression caused by *chrdl1* knockdown. This implies that an overactive *Bmp* signaling due to the deficient antagonist is additionally controlled on the transcriptional level by a negative feedback mechanism (25,26). Moreover, using intracellular phospho-SMAD1/5 as functional BMP signaling read-out, we measure paradoxical and obviously pathological effects in association with the here reported *CHRD1* mutation. On the one side, the basal BMP signaling activity is elevated comparing XMC versus healthy state. On the other hand, the BMP signaling is less inducible in correlation with lower superficial and intracellular *BMPR1A* abundance

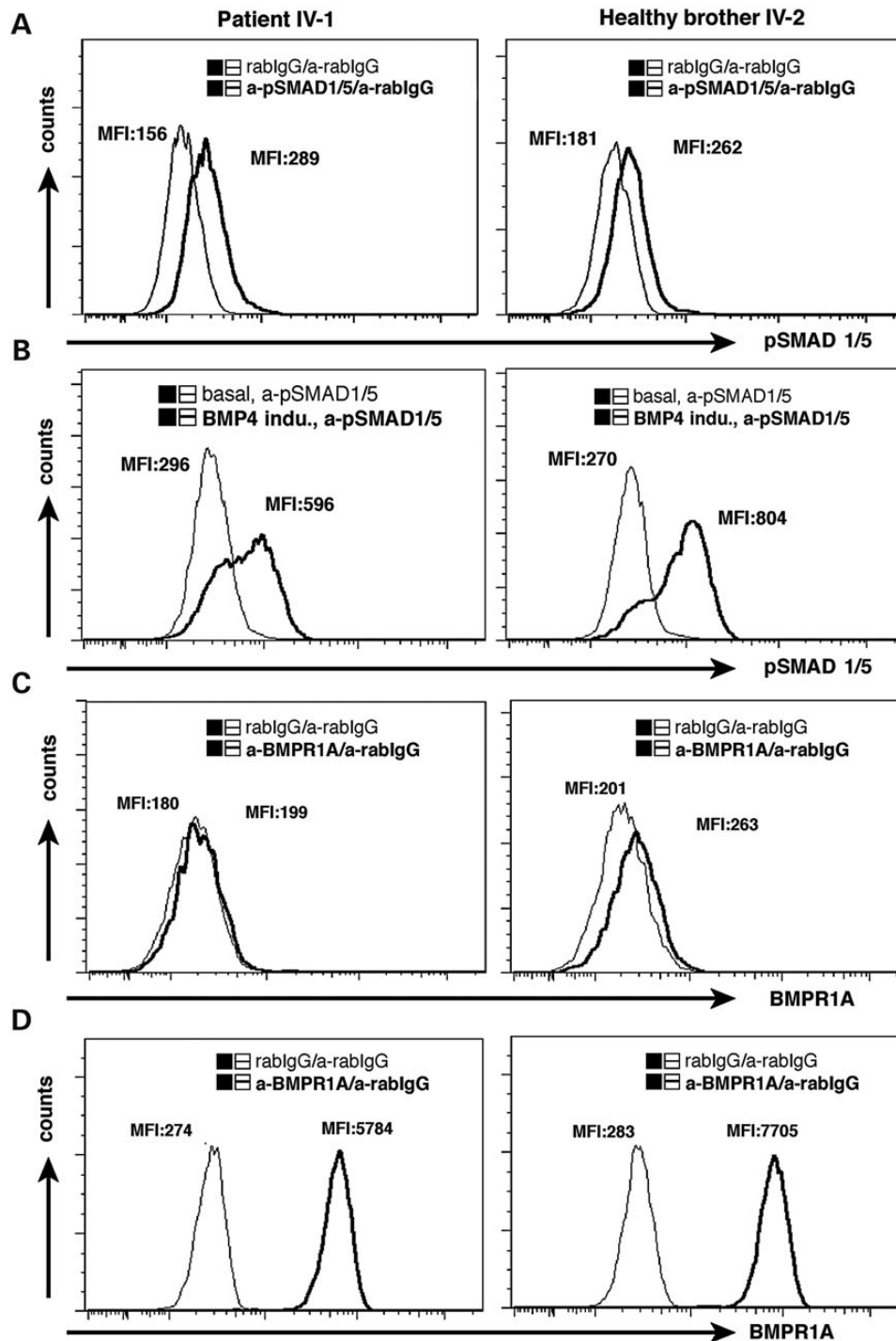


Figure 7. BMP signaling is altered in association with reported *CHRD1* mutation. BMP signaling was analyzed in lymphoblastoid cell lines of XMC patient IV-1 and his healthy brother IV-2 by flow-cytometry. Unprocessed MFIs are given for each specific staining and background measurement. (A) Basal level of intracellular pSMAD1/5. One representative experiment out of three is shown. (B) BMP4-induced intracellular pSMAD1/5. One representative experiment out of three is shown. (C) Surface and (D) intracellular staining of BMPR1A. One representative experiment out of two is shown.

comparing lymphoblastoid cells from XMC patient versus healthy brother. Together, we assume that the higher BMP signaling baseline in our XMC patient is the result from a failing BMP antagonism and consequently increased binding of BMP to BMPR1A. This induces a negative-feedback mechanism and leads to a compensatory down-regulation of BMP receptors (26). We assume that this kind of negative-feedback regulation

modifies the mutational outcome in a cell-dependent manner and can also be a reason for organ-specific manifestations and phenotypic variability.

Finally, the protein distribution pattern in our adult human cornea studies suggests that the developmentally important *CHRD1*-BMP4 antagonism could play a role in postnatal homeostasis of the cornea. We speculate that *CHRD1* acts as a stem cell

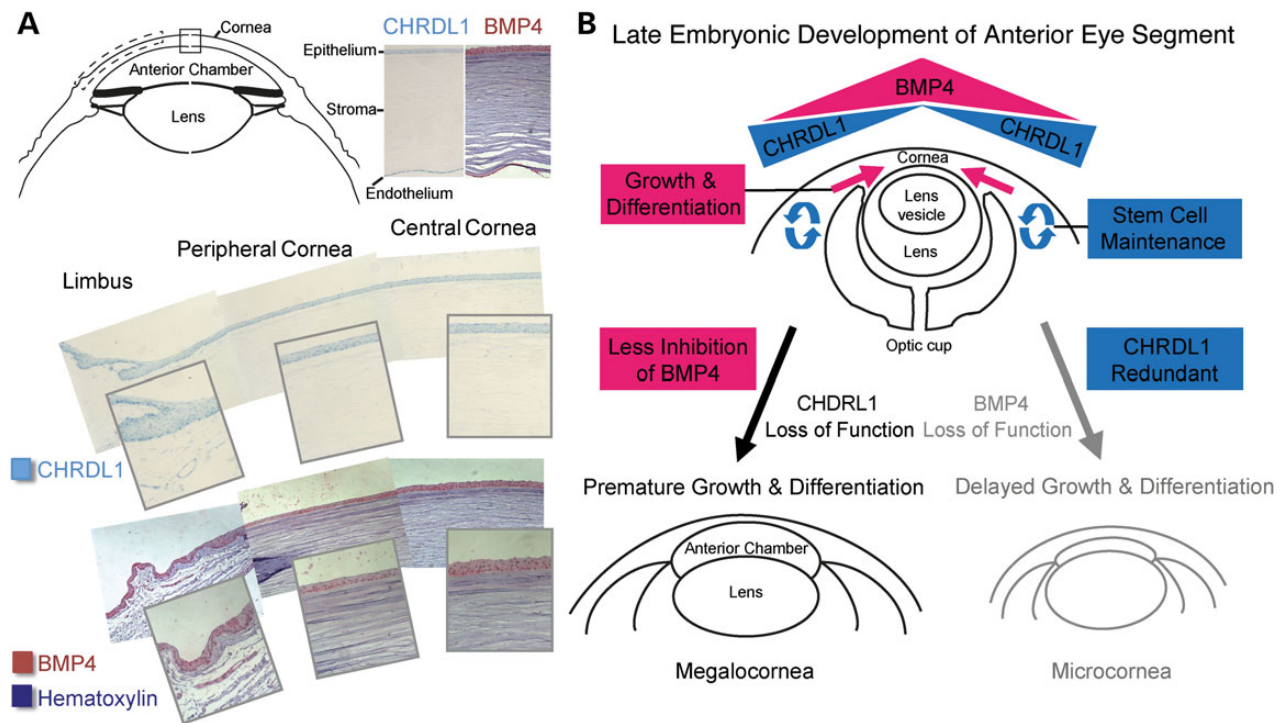


Figure 8. Protein expression of CHRDL1 and BMP4 in adult human cornea underlines their antagonistic function. (A) Immunohistochemistry of CHRDL1 (blue) and BMP4 (red) in healthy human cornea from anatomical sections. CHRDL1 is present in basal epithelial cells and stromal keratocytes of the limbus with decreasing protein levels centripetally. In contrast, BMP4 is homogeneously present in corneal epithelium and to a lesser extent in corneal stroma (bottom). Both proteins are also expressed in endothelium. Hematoxylin was used for counterstaining. (B) Model of molecular pathomechanism of megalocornea during late embryonic development of the anterior eye segment.

niche factor by attenuating the BMP4-mediated growth and differentiation, thereby preventing the exhaustion of the limbal stem cell pool. A similar role has been postulated for CHRDL1 in the intestinal stem cell niche (19). This concept is additionally supported by *in vitro* studies showing that the application of recombinant CHRDL1 inhibits differentiation and/or enhances proliferation of human mesenchymal stem cells and osteoblast precursor cell lines (25). Moreover, CHRDL1-mediated repression of BMP signaling leads to reactivation of embryonic homeobox genes like *MSX1* in immature lymphoblastic leukemia cells (T-ALL) (27,28).

In the case of superficial lesions, FGF2 signaling regulates the reconstitution of the cornea layers without fibrosis, while deep lesions lead to the activation of TGF β /BMP signaling in stromal keratocytes resulting in fibrosis (29). The increased expression of CHRDL1 in the stromal keratocytes of the corneal limbus suggests that CHRDL1 is also involved in repair mechanisms of the cornea.

Here, we propose a model, in which CHRDL1 influences BMP4 signaling to prevent fibrosis and limbal stem cell insufficiency, the latter often accompanied with irreversible lesions of the cornea. We suggest that CHRDL1 is a limbal stem cell niche factor and therefore an attractive target for regenerative medical therapies of corneal injuries.

Materials and Methods

Human and animal research

All subjects or their legal representatives gave written informed consent to the study, which was performed in accordance with

the Declaration of Helsinki. The informed-consent protocol for diagnostic genetic testing complies with the regulations of the German law for gene diagnostics (Gen-Diagnostik Gesetz). Cornea tissue samples were obtained from human anatomical sections performed at the Kantonsspital Basel (Switzerland) in accordance with the local ethics committee. All animal research procedures were performed according to guidelines set by the German animal use and care laws (Tierschutzgesetz) and approved by the German state administration Saxony-Anhalt (Projekt/AZ: 42502-3-600 MLU).

Ophthalmic examination

An ophthalmologist (P.R.) clinically assessed patients and their family members. Standard evaluation consisted of assessment of refraction anomalies and photographic documentation including scale-adjusted corneal diameter measurement, lateral view corneal profile and slit lamp findings. Measurement of the axial eye length and the AC depth was performed by optical interferometry (IOLMaster, Carl Zeiss Meditec). For corneal pachymetry, the Dual Scheimpflug Analyzer (Galilei) was used. Glaucoma in patients and their relatives were excluded by non-contact tonometry, stereoscopic evaluation of the optic nerve and confocal scanning laser ophthalmoscopy (HRT, Heidelberg Engineering) (30).

X-chromosomal exome capture and next-generation sequencing

Genomic DNA samples from the patients were extracted from ethylenediaminetetraacetic acid (EDTA) peripheral blood samples. We enriched the X-chromosomal exome from 4 μ g DNA of

Table 1. Comparison of etiology, phenotypes, management and prognosis of different disorders affecting cornea biometry

Differential diagnosis: altered corneal biometry	XMC/anterior megalophthalmos/megalocornea 1 [MIM309300] (1, 2,9)	Megalocornea with microspherophakia [MIM251750] allelic to primary congenital glaucoma 3D [MIM613086] (15,16)	Primary congenital glaucoma 3A [MIM231300]/open angle glaucoma 1A [MIM137750] (39–41)	Keratoconus [MIM148300]/keratoconus with cataract [MIM614303] (42–44)
Disease gene	CHRD1	LTBP2	CYP1B1, MYOC	VSX1, miR-184
Locus	Xq23	14q24.3	2p22.2, 1q24.3	20p11.21, 15q25.1
Inheritance	X-chromosomal recessive	Autosomal recessive	Autosomal recessive/dominant	Autosomal dominant
Diagnostic findings				
Corneal diameter	>12.5 mm	>12.5 mm	>12.5 mm (asymmetrical)	<12.5 mm
Corneal profile	Dome-shaped	Flat	Dome-shaped	Cone-shaped
AC	Deep	Deep/Flat	Deep	Normal
Pigment dispersion	Krukenberg spindle	Unknown	Sporadically present	Unknown
Lens shape	Normal	Spherophakia	Normal	Normal
Iris/ciliary ring	Enlarged + zonular weakness	Enlarged + zonular weakness	Primarily normal	Primarily normal
IOP	Primarily normal	Elevated in the case of lens dislocation	Primarily elevated	Primarily normal
Optic nerve cupping	Primarily normal	Primarily normal	Excavated	Normal
Medical implications				
Refraction anomalies	Mild myopia/astigmatism	Mild myopia/astigmatism	Primarily normal	Severe myopia/astigmatism
Lens luxation	Elevated risk	Highly elevated risk	No luxation	No luxation
Lens haze	Congenital cataract	Unknown	Unknown	Unknown
Corneal opacification	Mosaic corneal degeneration	Unknown	Descement-related	Unknown
Retinal detachment	Axial eye length-related	Unknown	Unknown	Unknown
Medical management				
Surgery	Electively: trabeculotomy, cataract surgery, keratoplasty	Electively/instantly: lens removal	Instantly: goniotomy	Contact lenses, cross-linking, electively keratoplasty
Follow-up	Regularly, long-term complication adjusted	Short intervals, short-term complication adjusted	Short intervals, short-term complication adjusted	Regularly, mid-term complication adjusted
Prognosis	Low to middle risk for vision impairment	Middle to high risk for vision impairment	Middle to high risk for vision impairment	Low to middle risk for vision impairment

patient III-5 using the Agilent SureSelect enrichment Kit according to the manufacturer's instructions. Single reads with a read length of 76 nucleotides were obtained by next-generation sequencing of one sample per lane with a mean coverage >30-fold on the Illumina Genome Analyzer Iix. The raw sequence data were aligned to the NCBI37/hg19 assembly of the human genome by Novoalign (31). Sequence variants were called by SAMtools and analyzed for an X-linked recessive inheritance mode using GeneTalk (32,33). Sequence variants with an allele frequency above 0.1% in healthy controls were removed and reduced to alleles with a predicted effect on the protein level (missense, stop-gain, stop-loss, frameshift, non-frameshift, splicing).

Validation of CHRD1 mutation by Sanger sequencing

PCR amplification and bidirectional sequencing of the identified CHRD1 mutation were performed using exon 9 forward 5'-CCA TGG CTA TGA CAA GAA CAA A-3' and reverse 5'-TCT TCC AAG CAA CTG CCT TT-3' primers according to the standard protocols. The sequence analysis was performed on an ABI3130xl capillary

sequencer (Applied Biosystems). Sequence data were processed using ABI software and were analyzed using Sequence Pilot (JSI medical systems GmbH) based on the complementary DNA (cDNA) reference sequence for CHRD1 (NM_001143981; ENST00000372042). The identified mutation was submitted to the public database ClinVar <http://www.ncbi.nlm.nih.gov/clinvar/> (ClinVar Accession SCV000195644, date last accessed, 20 February 2015).

Semi-quantitative RT-PCR

Peripheral blood samples were fractionated into MNC cells and granulocytes using the Ficoll-based standard protocol. RNA extraction was performed after cell lysis with TRIzol reagent (Invitrogen, Carlsbad, CA, USA) according to the phenol-chloroform standard protocol. Approximately 500 ng of RNA was extracted and reversely transcribed into cDNA with oligo-dT primers using MMLV RT (Life Technologies, USA). The CHRD1 exon-spanning PCR was performed with exon 2 forward primer 5'-AAG GAG GCA AAA ACA GAG CAA-3' and exon 3 reverse primer 5'-AAC CAA CCC ATA AGG TTC CA-3'. The PCR products were visualized by

running a 2% agarose gel with a mix molecular weight marker (NEB), staining with ethidium bromide and photo documentation under an UV transilluminator.

LCL culture and treatment with BMPs

Lymphoblastoid cell lines were generated from peripheral blood MNC cells according to a previously described protocol (34). LCLs from XMC patient IV-1 and his healthy brother IV-2 were kept in the Roswell Park Memorial Institute medium supplemented with 10% fetal calf serum (FCS), 1% penicillin/streptomycin and 1% glutamine. Stimulation with 125 ng/ml recombinant human BMP2 (355-BM-010, R&D Systems, Germany) or 100 ng/ml recombinant human BMP4 (314-BP-010, R&D Systems, Germany) was performed on 5×10^5 LCLs /well in 24-well plates for 24 h.

Flow cytometry

Flow cytometric analyses for surface receptor expression on live cells and for intracellular components on fixed/permeabilized cells were essentially performed as recently described (35). Briefly, 1×10^5 cells were stained with specific antibodies in fluorescence-activated cell sorting (FACS) buffer [phosphate-buffered saline (PBS) with 1% FCS and 0.3 mM EDTA]. Prior to specific antibody staining with anti-BMPR1A (ab38560, abcam, UK) and secondary anti-rabbit IgG-Alexa488 (A-11034, Invitrogen) on live cells, treatment with Fc γ block for 10 min on ice was performed. For live cell analyses, dead cells were excluded using PI staining. For intracellular analyses, cells were fixed for 10 min at 37°C with 4% paraformaldehyde. Followed by two washing steps, cells were permeabilized with 90% methanol buffer for 30 min on ice. Prior to specific antibody staining with anti-phospho-SMAD1/5 (Ser463/465) (13820P, Cell Signaling, USA) and anti-rabbit IgG-Alexa488 in FACS buffer, cells were incubated with Fc γ block for 15 min. Flow cytometry was performed using LSR Fortessa™ (Becton Dickinson) flow cytometer and FACS-Diva™ and FlowJo™ (Tree Star) software. To compare the protein levels between individuals, we calculated *delta mean fluorescence intensities* Δ MFI, meaning the subtraction of background MFI from specific MFI.

Immunohistochemistry

To investigate the physiological protein expression pattern of CHRDL1 (Ventroptin) and BMP4 in the human anterior eye segment, paraffin-embedded ophthalmic tissues were analyzed by immunostaining. We used a polyclonal rabbit anti-CHRDL1 antibody (HPA000250, ATLAS, Sweden) and a polyclonal rabbit anti-BMP4 antibody (ab39973, abcam) diluted 1:2000, respectively. Secondary Biotin-labeled anti-rabbit antibodies as diluted by the manufacturer (KPL, USA) were incubated and detected by Streptavidin-conjugated horseradish peroxidase using TrueBlue™ (CHRDL1) or Vectorred (BMP4) as a substrate.

Organisms and maintenance

Frogs (Xl) were obtained from commercial suppliers (NASCO, USA). Production and rearing of embryos was performed as described previously (36) and embryos were maintained at 15°C and staged according to NF.

Xl histology

For the preparation of vibratome sections, stained and fixed embryos were equilibrated in PBS containing 4.4 mg/ml gelatin, 0.27 g/ml bovine serum albumin and 0.18 g/ml sucrose. After

equilibration, embryos were mounted by cross-linking the solution with glutaraldehyde. 30 μ m sections were obtained with a Vibratome and mounted onto gelatin-coated slides. Photographs were taken on a Zeiss Imager M1 using Nomarski interference optics.

WMISH and RT-PCR

To analyze the spatiotemporal expression of *chr11* during Xl embryogenesis, a DIG-labeled 'antisense' RNA probe was generated by linearizing with Hind3-HF (NEB) and *in vitro* transcription with T7 RNA polymerase (Roche) as described before (37). *Xenopus* embryos were fixed at different developmental stages and whole-mount *in situ* hybridization was carried out as described previously (38). Embryos probed with antisense RNAs of *chr11* were vibratome sectioned (30 μ m) and photographed. RT-PCR was performed with the following intron spanning primers to amplify both possible *chr11* transcript variants scaffold71612 and scaffold10201, as annotated in Xenbase: *chr11*fwd-RT 5'-CTA GAG CCC TAT GGC CTT G-3', *chr11*rev-RT 5'-TGG TTC GTG ATG CTC CCA G-3', *odcfwd*-RT 5'-GCC ATT GTG AAG ACT CTC TCC ATT C-3', *odcrev*-RT 5'-TTC GGG TGA TTC CTT GCC AC-3'.

Xl knockdown experiments

25-mer MOs (Gene Tools, LLC Philomath, Oregon) were designed to target the splice site between Exon1 and Intron1 (MO1: 5'-ATC GAA ATG ATA TTA CCT CTC GGC A-3') or between Intron1 and Exon2 (MO2: 5'-CCA CCC TGA AAG ATA AAT CTC ACA T-3') in *chr11* mRNA transcripts. A mismatch standard MO was used as control (5'-CCT CTT ACC TCA GTT ACA ATT TAT A-3'). To measure the silencing efficiency by RT-PCR (see the above-mentioned primer pair), 2.5 pmol of either the *chr11* MO1 + 2 mixture or standard MO was injected into both blastomeres of 2-cell stage embryos, grown and collected at NF-stage 42. For unilateral knockdown experiments, we injected either the *chr11* MO1 + 2 mixture or the standard MO into one blastomere of 2-cell stage embryos. For statistical analysis of the differing eye phenotype between both injection categories, we used the χ^2 test including a total number of 384 embryos from three independent clutches. For biometric comparison of individual Xl eyes (injected side versus non-injected side), we calculated the mean value of both indicated diameters that are orthogonal to each other. We implemented the mean values of nine animals for statistical analysis using the one-tailed t-test.

Supplementary Material

Supplementary Material is available at HMG online.

Acknowledgements

We would like to thank the study family for their collaboration and contribution to this project. We thank Ute Spiekerkoetter (Center for Pediatrics and Adolescent Medicine, University Hospital of Freiburg), Matthew Warman, Justin Allen (Orthopaedic Research Laboratories, Boston Children's Hospital) and Claus-Eric Ott (Institute of Medical Genetics and Human Genetics, Charité Universitätsmedizin Berlin) for constant interest and support and for providing reagents. We acknowledge Fabienne Trotier and Randi Koll (Institute of Medical and Human Genetics, Charité Universitätsmedizin Berlin) for excellent technical assistance.

Conflict of Interest statement. None declared.

Funding

This work was supported by the B-Braun-Stiftung (Melsungen, Germany). We acknowledge for funding this work. The funders had no role in study design, data collection and analysis, decision to publish or preparation of the manuscript.

References

- Mackey, D.A., Buttery, R.G., Wise, G.M. and Denton, M.J. (1991) Description of X-linked megalocornea with identification of the gene locus. *Arch. Ophthalmol.*, **109**, 829–833.
- Meire, F.M. and Delleman, J.W. (1994) Biometry in X linked megalocornea: pathognomonic findings. *Br. J. Ophthalmol.*, **78**, 781–785.
- Davidson, A.E., Cheong, S.S., Hysi, P.G., Venturini, C., Plagnol, V., Ruddle, J.B., Ali, H., Carnt, N., Gardner, J.C., Hassan, H. et al. (2014) Association of CHRDL1 mutations and variants with X-linked megalocornea, Neuhauser syndrome and central corneal thickness. *PLoS One*, **9**, e104163.
- Mattos, A.M., Marques, A.D., Parrela, C.P., Fish, J.M., Artigalás, O.A., Ranzan, J., Winkler, M.I., Ohlweiler, L. and Riesgo Rdos, S. (2010) MMMM syndrome (macrocephaly, megalocornea, motor and mental retardation) and refractory epilepsy. *Arq. Neuropsiquiatr.*, **68**, 642–644.
- Pelit, A. and Akova, Y.A. (2005) Spontaneous posterior dislocation of both lenses in a patient with Marfan's syndrome: 17 years without complications. *Int. Ophthalmol.*, **26**, 49–51.
- Richter, C.U., Richardson, T.M. and Grant, W.M. (1986) Pigmentary dispersion syndrome and pigmentary glaucoma. A prospective study of the natural history. *Arch. Ophthalmol.*, **104**, 211–215.
- Siddiqui, Y., Ten Hulzen, R.D., Cameron, J.D., Hodge, D.O. and Johnson, D.H. (2003) What is the risk of developing pigmentary glaucoma from pigment dispersion syndrome? *Am. J. Ophthalmol.*, **135**, 794–799.
- Han, J., Young, J.W., Frausto, R.F., Isenberg, S.J. and Aldave, A.J. (2013) X-linked megalocornea associated with the novel CHRDL1 gene mutation p.(Pro56Leu*8). *Ophthalmic Genet.* [Epub ahead of print].
- Webb, T.R., Matarin, M., Gardner, J.C., Kelberman, D., Hassan, H., Ang, W., Michaelides, M., Ruddle, J.B., Pennell, C.E., Yazar, S. et al. (2012) X-linked megalocornea caused by mutations in CHRDL1 identifies an essential role for ventroptin in anterior segment development. *Am. J. Hum. Genet.*, **90**, 247–259.
- Sakuta, H., Suzuki, R., Takahashi, H., Kato, A., Shintani, T., Iemura, S., Yamamoto, T.S., Ueno, N. and Noda, M. (2001) Ventroptin: a BMP-4 antagonist expressed in a double-gradient pattern in the retina. *Science*, **293**, 111–115.
- Ouyang, H., Xue, Y., Lin, Y., Zhang, X., Xi, L., Patel, S., Cai, H., Luo, J., Zhang, M., Zhang, M. et al. (2014) WNT7A and PAX6 define corneal epithelium homeostasis and pathogenesis. *Nature*, **511**, 358–361.
- Ksander, B.R., Kolovou, P.E., Wilson, B.J., Saab, K.R., Guo, Q., Ma, J., McGuire, S.P., Gregory, M.S., Vincent, W.J., Perez, V.L. et al. (2014) ABCB5 is a limbal stem cell gene required for corneal development and repair. *Nature*, **511**, 353–357.
- Coffinier, C., Tran, U., Larrain, J. and De Robertis, E.M. (2001) Neuralin-1 is a novel Chordin-related molecule expressed in the mouse neural plate. *Mech. Dev.*, **100**, 119–122.
- Ahmadiéh, H., Banaee, T., Javadi, M.A., Jafarinasab, M.R., Yazdani, S. and Sajjadi, H. (2006) Vitreoretinal disorders in anterior megalophthalmos. *Jpn. J. Ophthalmol.*, **50**, 515–523.
- Desir, J., Sznajder, Y., Depasse, F., Roulez, F., Schrooyen, M., Meire, F. and Abramowicz, M. (2010) LTBP2 null mutations in an autosomal recessive ocular syndrome with megalocornea, spherophakia, and secondary glaucoma. *Eur. J. Hum. Genet.*, **18**, 761–767.
- Khan, A.O., Aldahmesh, M.A. and Alkuraya, F.S. (2011) Congenital megalocornea with zonular weakness and childhood lens-related secondary glaucoma - a distinct phenotype caused by recessive LTBP2 mutations. *Mol. Vis.*, **17**, 2570–2579.
- Nagy, E. and Maquat, L.E. (1998) A rule for termination-codon position within intron-containing genes: when nonsense affects RNA abundance. *Trends Biochem. Sci.*, **23**, 198–199.
- Miller, J.N. and Pearce, D.A. (2014) Nonsense-mediated decay in genetic disease: friend or foe? *Mutat. Res. Rev. Mutat. Res.*, **762**, 52–64.
- Kosinski, C., Li, V.S., Chan, A.S., Zhang, J., Ho, C., Tsui, W.Y., Chan, T.L., Mifflin, R.C., Powell, D.W., Yuen, S.T. et al. (2007) Gene expression patterns of human colon tops and basal crypts and BMP antagonists as intestinal stem cell niche factors. *Proc. Natl Acad. Sci. USA*, **104**, 15418–15423.
- Collinson, J.M., Hill, R.E. and West, J.D. (2004) Analysis of mouse eye development with chimeras and mosaics. *Int. J. Dev. Biol.*, **48**, 793–804.
- Cvekl, A. and Tamm, E.R. (2004) Anterior eye development and ocular mesenchyme: new insights from mouse models and human diseases. *Bioessays*, **26**, 374–386.
- Bakrania, P., Efthymiou, M., Klein, J.C., Salt, A., Bunyan, D.J., Wyatt, A., Ponting, C.P., Martin, A., Williams, S., Lindley, V. et al. (2008) Mutations in BMP4 cause eye, brain, and digit developmental anomalies: overlap between the BMP4 and hedgehog signaling pathways. *Am. J. Hum. Genet.*, **82**, 304–319.
- Reis, L.M., Tyler, R.C., Schilter, K.F., Abdul-Rahman, O., Innis, J.W., Kozel, B.A., Schneider, A.S., Bardakjian, T.M., Lose, E.J., Martin, D.M. et al. (2011) BMP4 loss-of-function mutations in developmental eye disorders including SHORT syndrome. *Hum. Genet.*, **130**, 495–504.
- Rainger, J., van Beusekom, E., Ramsay, J.K., McKie, L., Al-Gazali, L., Pallotta, R., Saponari, A., Branney, P., Fisher, M., Morrison, H. et al. (2011) Loss of the BMP antagonist, SMOC-1, causes Ophthalmic-acromelic (Waardenburg Anophthalmia) syndrome in humans and mice. *PLoS Genet.*, **7**, e1002114.
- Nicklas, D. and Saiz, L. (2013) Characterization of negative feedback network motifs in the TGF-beta signaling pathway. *PLoS One*, **8**, e83531.
- Sun, Q., Mao, S., Li, H., Zen, K., Zhang, C.Y. and Li, L. (2013) Role of miR-17 family in the negative feedback loop of bone morphogenetic protein signaling in neuron. *PLoS One*, **8**, e83067.
- Fernandes, H., Dechering, K., van Someren, E., Steeghs, I., Apothecker, M., Mentink, A., van Blitterswijk, C. and de Boer, J. (2010) Effect of chordin-like 1 on MC3T3-E1 and human mesenchymal stem cells. *Cells Tissues Organs*, **191**, 443–452.
- Nagel, S., Ehrentraut, S., Meyer, C., Kaufmann, M., Drexler, H.G. and MacLeod, R.A. (2015) Repressed BMP signaling reactivates NKX homeobox gene MSX1 in a T-ALL subset. *Leuk. Lymphoma*, **56**, 480–491.
- Jester, J.V. and Ho-Chang, J. (2003) Modulation of cultured corneal keratocyte phenotype by growth factors/cytokines control in vitro contractility and extracellular matrix contraction. *Exp. Eye Res.*, **77**, 581–592.
- Wollstein, G., Garway-Heath, D.F. and Hitchings, R.A. (1998) Identification of early glaucoma cases with the scanning laser ophthalmoscope. *Ophthalmology*, **105**, 1557–1563.
- Hercus, C. (2011) www.novocraft.com (date last accessed, 20 February 2015).

32. Li, H., Handsaker, B., Wysoker, A., Fennell, T., Ruan, J., Homer, N., Marth, G., Abecasis, G. and Durbin, R. (2009) The sequence alignment/map format and SAMtools. *Bioinformatics*, **25**, 2078–2079.
33. Kamphans, T. and Krawitz, P.M. (2012) GeneTalk: an expert exchange platform for assessing rare sequence variants in personal genomes. *Bioinformatics*, **28**, 2515–2516.
34. Neitzel, H. (1986) A routine method for the establishment of permanent growing lymphoblastoid cell lines. *Hum. Genet.*, **73**, 320–326.
35. Quandt, D., Fiedler, E., Boettcher, D., Marsch, W. and Seliger, B. (2011) B7-h4 expression in human melanoma: its association with patients' survival and antitumor immune response. *Clin. Cancer Res.*, **17**, 3100–3111.
36. Pfirrmann, T., Lokapally, A., Andreasson, C., Ljungdahl, P. and Hollemann, T. (2013) SOMA: a single oligonucleotide mutagenesis and cloning approach. *PLoS One*, **8**, e64870.
37. Cornesse, Y., Pieler, T. and Hollemann, T. (2005) Olfactory and lens placode formation is controlled by the hedgehog-interacting protein (Xhip) in *Xenopus*. *Dev. Biol.*, **277**, 296–315.
38. Hollemann, T., Bellefroid, E. and Pieler, T. (1998) The *Xenopus* homologue of the *Drosophila* gene *tailless* has a function in early eye development. *Development*, **125**, 2425–2432.
39. Bejjani, B.A., Lewis, R.A., Tomey, K.F., Anderson, K.L., Dueker, D.K., Jabak, M., Astle, W.F., Otterud, B., Leppert, M. and Lupski, J.R. (1998) Mutations in CYP1B1, the gene for cytochrome P4501B1, are the predominant cause of primary congenital glaucoma in Saudi Arabia. *Am. J. Hum. Genet.*, **62**, 325–333.
40. Stoilov, I., Akarsu, A.N. and Sarfarazi, M. (1997) Identification of three different truncating mutations in cytochrome P4501B1 (CYP1B1) as the principal cause of primary congenital glaucoma (Buphthalmos) in families linked to the GLC3A locus on chromosome 2p21. *Hum. Mol. Genet.*, **6**, 641–647.
41. Stone, E.M., Fingert, J.H., Alward, W.L., Nguyen, T.D., Polansky, J.R., Sunden, S.L., Nishimura, D., Clark, A.F., Nystuen, A., Nichols, B.E. et al. (1997) Identification of a gene that causes primary open angle glaucoma. *Science*, **275**, 668–670.
42. Dash, D.P., George, S., O'Prey, D., Burns, D., Nabili, S., Donnelly, U., Hughes, A.E., Silvestri, G., Jackson, J., Frazer, D. et al. (2010) Mutational screening of VSX1 in keratoconus patients from the European population. *Eye (Lond.)*, **24**, 1085–1092.
43. Fadlallah, A., Dirani, A., El Rami, H., Cherfane, G. and Jarade, E. (2013) Safety and visual outcome of Visian toric ICL implantation after corneal collagen cross-linking in keratoconus. *J. Refract. Surg.*, **29**, 84–89.
44. Hughes, A.E., Bradley, D.T., Campbell, M., Lechner, J., Dash, D.P., Simpson, D.A. and Willoughby, C.E. (2011) Mutation altering the miR-184 seed region causes familial keratoconus with cataract. *Am. J. Hum. Genet.*, **89**, 628–633.